Sensitivity Analysis of Lumped-Parameter Thermal Networks for the Experimental Calibration of eMotor Models

Jon García Urbieta, Borja Rodríguez, Antonio J. Rodríguez, Pablo Díaz, Sergio Armentia, Francisco González

This is a post-peer-review, pre-copyedit version of an article published in IEEE Transactions on Transportation Electrification. The final authenticated version is available online at: http://dx.doi.org/10.1109/TTE.2023.3331097.

Sensitivity Analysis of Lumped-Parameter Thermal Networks for the Experimental Calibration of eMotor Models

Jon García Urbieta, Borja Rodríguez, Antonio J. Rodríguez, Pablo Díaz, Sergio Armentia, Francisco González

***Abstract*—Lumped-parameter thermal networks (LPTNs) are efficient computational models that can be used to replicate the thermal behavior of eMotors in a way that is compatible with real-time execution. The accuracy of the simulation results delivered by LPTNs relies on the selection of an appropriate topology and the accurate tuning of their parameters, namely resistances, capacities and heat sources. It is difficult, however, to obtain an accurate tuning of the parameters starting from theoretical expressions, and these often need to be adjusted based on experimental calibration. Several methods can be used to this end; among these, finite differences are a popular option. This paper presents a methodology for the analytical determination of the sensitivity of LPTN dynamics with respect to its lumped parameters. The obtained analytical sensitivities provide information about the effect of the circuit parameters on the thermal dynamics of the overall system, and can be used to enable the use of gradient-based optimization methods to adjust the LPTN parameters. The proposed method overcomes several limitations of finite difference approaches, like the computational load incurred when the number of parameters to be adjusted is large, and the variability of the results with the increment used to define the finite differences. The analytical sensitivities were tested in the analysis and optimization of a benchmark thermal model and the LPTN representation of a permanent-magnet synchronous motor.**

***Index Terms*—Lumped-parameter thermal network, sensitivity analysis, parameter calibration, thermal management, eMotor, ePowertrain.**

I. Introduction

THERMAL effects play a critical role in the operation of ePowertrains. Components such as eMotors and inverters can have their performance compromised by the accumulation of heat; high temperatures can also result in a relevant shortening of their useful life if certain thresholds are exceeded [1]. This is the case of permanent-magnet synchronous motors (PMSMs), the most frequently used type of electric drive in automotive ePowertrains: excessive temperature can cause permanent damage to the motor magnets, rendering them useless in extreme cases [2], [3]. Moreover, the accumulation of thermal cycling also affects PMSMs irreversibly, and the resulting thermal aging gives rise to the degradation of the motor properties over time [4], [5]. On the other hand, the optimal operation of electric drives requires them to perform as close as possible to their admissible temperature limits. Attaining this goal requires an accurate knowledge of the internal temperatures and heat flows of the motor, in order to define control algorithms to regulate the operation of the drive or to be able to predict the evolution of the thermal point of the device during a given manoeuvre.

The thermal dynamics of ePowertrain devices can be described by means of numerical methods such as computational fluid dynamics and finite elements [6], [5], [7]. While these representations are often detailed and accurate, they are computationally expensive and cannot be used in real-time applications. Lumped-parameter thermal networks (LPTNs) are an alternative modelling approach based on the concentration of the thermal properties of the system in discrete elements, similar to those used in an electric circuit. Thermal descriptions based on LPTNs are computationally efficient and can deliver real-time execution, even when deployed on hardware architectures with limited resources [8]. This favourable trade-off between temperature estimation accuracy and computational resources makes them the option of choice for monitoring algorithms, e.g., those based on state estimation from sensor readings through Kalman filtering [9], [10], [11]. However, the use of LPTNs to describe the thermal behaviour of a system requires the consideration of several issues. First, although different levels of complexity of the representation can be used, the thermal dynamics of the physical device are simplified when using LPTNs. The selection of an appropriate topology is necessary for the predicted dynamics to correspond to that of the modelled system. Besides, the parameters of the thermal circuit need to be carefully adjusted to match the system dynamics; theoretical expressions can be used to this end but, in practice, a tuning step based on experimental results is often needed. Consistently, the selected parameters are the ones that present ambivalence and that usually do not interfere with the physical sense of the model. Some examples are the characterization of the impregnation goodness in the winding slot, convection heat transfer coefficients, stator-housing interference gaps, orthotropic properties, and cooling parameters, among others [12], [13].

Determining appropriate parameters for an LPTN representation can be addressed in several ways. Uncertain parameters

J. García Urbieta, B. Rodríguez, and S. Armentia are with GKN Automotive Zumaia, 20750 Zumaia, Spain (e-mail: {jon.garcia, borja.rodriguez, sergio.armentia}@gknautomotive.com). A. J. Rodríguez, P. Díaz, and F. González are with Laboratorio de Ingeniería Mecánica at CITENI, Campus Industrial Ferrol, University of A Coruña, 15403 Ferrol, Spain (e-mail: {f.gonzalez, antonio.rodriguez.gonzalez@udc.es, pablo.diaz.brage@udc.es}@udc.es).

(Corresponding author: Jon García Urbieta):

This research was funded by the Ministry of Economy of Spain through the Ramón y Cajal programme, grant number RYC-2016-20222, and the Galician Government through grants ED431B2016/031 and ED431F2021/04.

can be estimated by means of global identification methods [14] or using extended Kalman filters [11]. Sensitivity analysis is frequently used as tuning strategy, e.g., [15], [13], [16]. In most cases, a finite differences approach is adopted, in which a forward-dynamics simulation is repeated several times after selected parameters have been perturbed. This solution enables one to obtain an approximation of the sensitivity of the system dynamics with respect to these parameters, that can be used to identify the most critical ones and focus the optimization effort on them. The computational workload of finite-difference based sensitivity analysis, however, increases considerably when the number of parameters under study is large [15]. Additionally, it can lead to inaccurate results if the selection of the perturbation size is not carefully performed [17], although this problem can be alleviated through the use of complex-step differentiation [18]. Another option to evaluate the system sensitivity is employing automatic differentiation (AD) methods, based on decomposing computations into elemental mathematical operations with known direct analytical derivatives [19], [20], [21].

This work describes a methodology for the evaluation of the sensitivity of LPTNs based on the analytical differentiation of the circuit dynamics, an approach that delivers both fast and accurate solutions thanks to the computation of the exact derivatives of the original equations. The proposed solution is similar to the direct differentiation strategies that exist in the field of multibody system dynamics, e.g., [22]. The method is based on the analytical differentiation of the dynamics equations with respect to the system parameters, in order to obtain the sensitivities of the variables that describe the circuit state. The evaluation of these sensitivities is conducted after the completion of each integration time step of the LPTN dynamics through the solution of a system of linear equations, which results in a moderate overhead in terms of the overall time elapsed in computations. The resulting sensitivities can be used as input for gradient-based optimization methods, and thus be used to adjust the LPTN parameters, for instance in the calibration of the model from experimental measurements.

This new sensitivity analysis method was assessed in the study of a benchmark problem and the calibration of the LPTN of an automotive-grade PMSM from test bench measurements. Results confirmed that the analytical sensitivities accurately reflect the effect of the circuit parameters on the temperatures and heat flows of the system, and that they can be used to optimize model definition by means of gradient-based methods in a computationally efficient fashion.

II. Modelling and sensitivity analysis methods

Lumped-parameter thermal networks enable the expression of the thermal dynamics of a physical system by means of equations similar to those used to describe electric circuits. These equations can be formulated in different ways; here we are following the approach put forward in [8], in which the system dynamics is described using a set of n variables $\mathbf{x}$ that includes n_T node temperatures and n_Q heat flows through components, grouped in terms $\mathbf{x}_T$ and $\mathbf{x}_Q$, respectively:

$$\mathbf{x} = \left[\begin{array}{cc} \mathbf{x}_T{}^{\mathrm{T}} & \mathbf{x}_Q{}^{\mathrm{T}} \end{array} \right]^{\mathrm{T}} \tag{1}$$

The definition of the LPTN also includes a set of r parameters $\boldsymbol{\rho}$ that represent the thermal properties of the components and their operation conditions. The variables in (1) are not independent. They are constrained by Kirchhoff's laws and the constitutive equations of the circuit components, which impose a total of m algebraic constraints on $\mathbf{x}$ that can be generally written in the form

$$\boldsymbol{\Phi}\left(\mathbf{x}, \boldsymbol{\rho}, t\right) = \mathbf{0} \tag{2}$$

Some system components, namely thermal capacitors, also subject the variables $\mathbf{x}$ to a set of p first-order ordinary differential equations (ODEs), which can be expressed as

$$\boldsymbol{\Gamma}\left(\mathbf{x}, \dot{\mathbf{x}}, \boldsymbol{\rho}, t\right) = \mathbf{A}\left(\mathbf{x}, \boldsymbol{\rho}, t\right)\dot{\mathbf{x}} + \mathbf{b}\left(\mathbf{x}, \boldsymbol{\rho}, t\right) = \mathbf{0} \tag{3}$$

where $\mathbf{A}$ and $\mathbf{b}$ are $p \times n$ and $p \times 1$ terms, respectively. System solvability often requires that $n = p + m$.

The direct sensitivity analysis of the system requires the numerical integration of the LPTN dynamics prior to the evaluation of sensitivity quantities. The dynamic formulation used to this end is presented next.

A. Dynamic formulation

Together, (2) and (3) completely describe the system dynamics as a set of differential-algebraic equations (DAEs):

$$\left[\begin{array}{c} \boldsymbol{\Phi} \\ \mathbf{A}\dot{\mathbf{x}} + \mathbf{b} \end{array} \right] = \mathbf{0} \tag{4}$$

The forward-dynamics simulation of the LPTN response requires the solution of the nonlinear system (4), in which both $\mathbf{x}$ and $\dot{\mathbf{x}}$ are unknowns. This can be achieved introducing a numerical integration formula in (4) to make the dynamic equilibrium explicitly dependent on the variables $\mathbf{x}$ at time-step $k+1$, but not on their derivatives $\dot{\mathbf{x}}$,

$$\mathbf{f}\left(\mathbf{x}^{k+1}\right) = \mathbf{0} \tag{5}$$

In (5), the system variables at time-step $k+1$ are the only unknowns. The system can be solved by means of Newton-Raphson iteration

$$\left[\frac{\mathrm{d}\mathbf{f}\left(\mathbf{x}\right)}{\mathrm{d}\mathbf{x}} \right]_i \Delta\mathbf{x}_{i+1} = -\left[\mathbf{f}\left(\mathbf{x}\right) \right]_i \tag{6}$$

$$\mathbf{x}_{i+1} = \mathbf{x}_i + \Delta\mathbf{x}_{i+1} \tag{7}$$

where the subscript i stands for the iteration number.

Backward differentiation formulas (BDF) are used here as numerical integrator [23]. These express the derivatives of the system variables at time-step $k+1$ as

$$\begin{aligned} \dot{\mathbf{x}}^{k+1} &= -\frac{1}{h}\sum_{j=0}^{\hat{k}} \alpha_j \mathbf{x}^{k+1-j} \\ &= -\frac{1}{h}\left(\alpha_0 \mathbf{x}^{k+1} + \sum_{j=1}^{\hat{k}} \alpha_j \mathbf{x}^{k+1-j}\right) \\ &= -\frac{1}{h}\left(\alpha_0 \mathbf{x}^{k+1} + \hat{\mathbf{x}}^{k}\right) \end{aligned} \tag{8}$$

where h is the integration step-size and α_j $(j = 1, 2, \ldots, \hat{k})$ are scalar coefficients that depend on the BDF order $\hat{k}$, shown

TABLE I: Coefficients of BDF integration formulas

$\hat{k}$	α_0	α_1	α_2	α_3
1	-1	1	-	-
2	$-3/2$	2	$-1/2$	-
3	$-11/6$	3	$-3/2$	$1/3$

in Table I for orders 1 to 3. It must be noted that term $\hat{\dot{\mathbf{x}}}^k$ in (8) remains constant during the Newton-Raphson iteration process, as its value depends only on system variables already computed in previous integration steps.

Replacing the expression of the system derivatives $\dot{\mathbf{x}}$ with the integration formula in (8), the nonlinear system of equations to be solved in (5) becomes

$$\mathbf{f}\left(\mathbf{x}^{k+1}\right) = \left[\begin{array}{c} \mathbf{\Phi} \\ -\frac{1}{h}\mathbf{A}\left(\alpha_0\mathbf{x}^{k+1} + \hat{\dot{\mathbf{x}}}^k\right) + \mathbf{b} \end{array}\right]^{k+1} = \mathbf{0} \quad (9)$$

The corresponding tangent matrix required by (7) is

$$\frac{\mathrm{d}\mathbf{f}\left(\mathbf{x}\right)}{\mathrm{d}\mathbf{x}} = \left[\begin{array}{c} \mathbf{\Phi}_\mathbf{x} \\ -\frac{1}{h}\left(\alpha_0\mathbf{A} + \mathbf{A}_\mathbf{x}\left(\alpha_0\mathbf{x}^{k+1} + \hat{\dot{\mathbf{x}}}^k\right)\right) + \mathbf{b}_\mathbf{x} \end{array}\right] \quad (10)$$

where subscript $()_y = \partial()/\partial y$ indicates a partial derivative with respect to variable y.

B. Sensitivity analysis

The optimization problem of an LPTN consists of obtaining values of the system parameters $\boldsymbol{\rho}$ such that a certain set of conditions is satisfied during simulation. The satisfaction of these conditions can be expressed by means of cost or objective functions ψ, written in terms of the parameters, the system variables, and their derivatives as

$$\psi = w\left(\mathbf{x}^q, \dot{\mathbf{x}}^q, \boldsymbol{\rho}^q\right) + \int_{t^0}^{t^q} g\left(\mathbf{x}, \dot{\mathbf{x}}, \boldsymbol{\rho}\right)\mathrm{d}t \quad (11)$$

where w is the part of the cost function associated with the state of the system at final time t^q, and g is another part related to its transient response. Term t^0 stands for the initial time and superscript $()^q$ denotes values at t^q. The optimization can be performed using gradient methods, which require the evaluation of the gradient of the objective function with respect to the parameters as

$$\nabla_{\boldsymbol{\rho}}\psi^\mathrm{T} = \frac{\partial\psi}{\partial\boldsymbol{\rho}} = \psi_{\boldsymbol{\rho}} \quad (12)$$

Introducing (11) in (12), the gradient of the objective function is expressed as

$$\begin{aligned}\nabla_{\boldsymbol{\rho}}\psi^\mathrm{T} = &\left(w_\mathbf{x}\mathbf{x}_{\boldsymbol{\rho}} + w_{\dot{\mathbf{x}}}\dot{\mathbf{x}}_{\boldsymbol{\rho}} + w_{\boldsymbol{\rho}}\right) \\ &+ \int_{t^0}^{t^q}\left(g_\mathbf{x}\mathbf{x}_{\boldsymbol{\rho}} + g_{\dot{\mathbf{x}}}\dot{\mathbf{x}}_{\boldsymbol{\rho}} + g_{\boldsymbol{\rho}}\right)\mathrm{d}t\end{aligned} \quad (13)$$

In (13), the derivatives of functions w and g are known, because the objective function ψ is defined by the analyst. However, terms $\mathbf{x}_{\boldsymbol{\rho}}, \dot{\mathbf{x}}_{\boldsymbol{\rho}} \in \mathbb{R}^{n\times r}$ need to be determined. These are the matrices that provide the sensitivity of the variables and their derivatives with respect to the system parameters $\boldsymbol{\rho}$, and represent the unknowns that are obtained through the solution of the sensitivity problem.

In order to determine the sensitivities $\mathbf{x}_{\boldsymbol{\rho}}$ and $\dot{\mathbf{x}}_{\boldsymbol{\rho}}$, we start by highlighting the dependence of the system dynamics terms in (4) from the parameters $\boldsymbol{\rho}$, variables, and derivatives, rewriting the general problem statement as

$$\mathbf{f}\left(\mathbf{x}^{k+1}\right) = \left[\begin{array}{c} \mathbf{\Phi}\left(\mathbf{x}, \boldsymbol{\rho}, t\right) \\ \mathbf{\Gamma}\left(\mathbf{x}, \dot{\mathbf{x}}, \boldsymbol{\rho}, t\right) \end{array}\right]^{k+1} = \mathbf{0}_{n\times 1} \quad (14)$$

The differentiation of (14) with respect to the system parameters $\boldsymbol{\rho}$ results in

$$\begin{aligned}\frac{\mathrm{d}\mathbf{f}\left(\mathbf{x}^{k+1}\right)}{\mathrm{d}\boldsymbol{\rho}} &= \left[\begin{array}{c} \mathbf{\Phi}_\mathbf{x}\mathbf{x}_{\boldsymbol{\rho}} + \mathbf{\Phi}_{\boldsymbol{\rho}} \\ \left(\mathbf{A}_\mathbf{x}\mathbf{x}_{\boldsymbol{\rho}} + \mathbf{A}_{\boldsymbol{\rho}}\right)\dot{\mathbf{x}} + \mathbf{A}\dot{\mathbf{x}}_{\boldsymbol{\rho}} + \mathbf{b}_\mathbf{x}\mathbf{x}_{\boldsymbol{\rho}} + \mathbf{b}_{\boldsymbol{\rho}} \end{array}\right]^{k+1} \\ &= \mathbf{0}_{n\times r}\end{aligned} \quad (15)$$

Equation (15) describes a system of $n \times r$ linear equations in which the unknowns are $\mathbf{x}_{\boldsymbol{\rho}}$ and $\dot{\mathbf{x}}_{\boldsymbol{\rho}}$, known in the literature as Tangent Linear Model (TLM). The number of equations is not enough, however, to solve uniquely for $\mathbf{x}_{\boldsymbol{\rho}}$ and $\dot{\mathbf{x}}_{\boldsymbol{\rho}}$, as each of these unknown terms is of size $n \times r$. However, the system sensitivities $\mathbf{x}_{\boldsymbol{\rho}}^{k+1}$ and $\dot{\mathbf{x}}_{\boldsymbol{\rho}}^{k+1}$ can be related by means of a numerical integration formula. It is possible, but not strictly necessary, to use the same integrator that was selected for the dynamics; if this is the case, using the BDF formula leads to the relation

$$\dot{\mathbf{x}}_{\boldsymbol{\rho}}^{k+1} = -\frac{\alpha_0}{h}\mathbf{x}_{\boldsymbol{\rho}}^{k+1} - \frac{1}{h}\hat{\dot{\mathbf{x}}}_{\boldsymbol{\rho}}^k; \qquad \text{where } \hat{\dot{\mathbf{x}}}_{\boldsymbol{\rho}}^k = \sum_{j=1}^{\hat{k}}\alpha_j\mathbf{x}_{\boldsymbol{\rho}}^{k+1-j} \quad (16)$$

Term $\hat{\dot{\mathbf{x}}}_{\boldsymbol{\rho}}^k$ is known at time step $k+1$. Introducing the expression of the integrator (16) into the TLM (15) results in

$$\mathbf{\Phi}_\mathbf{x}\mathbf{x}_{\boldsymbol{\rho}}^{k+1} + \mathbf{\Phi}_{\boldsymbol{\rho}} = \mathbf{0} \quad (17a)$$

$$\begin{aligned}&\left(\mathbf{A}_\mathbf{x}\mathbf{x}_{\boldsymbol{\rho}}^{k+1} + \mathbf{A}_{\boldsymbol{\rho}}\right)\dot{\mathbf{x}}^{k+1} - \frac{\alpha_0}{h}\mathbf{A}\mathbf{x}_{\boldsymbol{\rho}}^{k+1} \\ &- \frac{1}{h}\mathbf{A}\hat{\dot{\mathbf{x}}}_{\boldsymbol{\rho}}^k + \mathbf{b}_\mathbf{x}\mathbf{x}_{\boldsymbol{\rho}}^{k+1} + \mathbf{b}_{\boldsymbol{\rho}} = \mathbf{0}_{n\times r}\end{aligned} \quad (17b)$$

The product $\mathbf{A}_\mathbf{x}\mathbf{x}_{\boldsymbol{\rho}}\dot{\mathbf{x}}$ can be rewritten using tensor-matrix product rules as $\left(\mathbf{A}_\mathbf{x}\dot{\mathbf{x}}\right)\mathbf{x}_{\boldsymbol{\rho}}$, in which the hypermatrix $\mathbf{A}_\mathbf{x}$ is considered as a stack of two-dimensional matrices. This makes it possible to express system (17) in the form

$$\mathbf{M}\mathbf{x}_{\boldsymbol{\rho}}^{k+1} = \mathbf{m} \quad (18)$$

with

$$\mathbf{M} = \left[\begin{array}{c} \mathbf{\Phi}_\mathbf{x} \\ \mathbf{A}_\mathbf{x}\dot{\mathbf{x}}^{k+1} - \frac{\alpha_0}{h}\mathbf{A} + \mathbf{b}_\mathbf{x} \end{array}\right] \quad (19)$$

$$\mathbf{m} = \left[\begin{array}{c} -\mathbf{\Phi}_{\boldsymbol{\rho}} \\ -\mathbf{A}_{\boldsymbol{\rho}}\dot{\mathbf{x}}^{k+1} + \frac{1}{h}\mathbf{A}\hat{\dot{\mathbf{x}}}_{\boldsymbol{\rho}}^k - \mathbf{b}_{\boldsymbol{\rho}} \end{array}\right] \quad (20)$$

Note that terms $\mathbf{x}$ and $\dot{\mathbf{x}}$ are already known at time t^{k+1}, because the evaluation of the sensitivities takes place after the solution of the system dynamics.

C. Initialization

The forward-dynamics simulation that results from the numerical integration of (4) needs to start from a set of variables $\mathbf{x}^0$ that is compatible with the algebraic constraints $\boldsymbol{\Phi} = \mathbf{0}$ in (2). The number of constraints, however, will be smaller than the number of variables ($m < n$) if the LPTN includes thermal capacitors, which do not introduce algebraic constraints but differential ones. In this case, it is necessary to specify the initial temperatures of these components by means of equations in the form $\xi_a = T_a - T_a^0 = 0$, where T_a is the temperature of the node to which the capacitor is connected, to arrive at a system of equations with a unique solution

$$\left[\begin{array}{c} \boldsymbol{\Phi} \\ \boldsymbol{\Xi} \end{array} \right]^0 = \mathbf{0} \tag{21}$$

where $\boldsymbol{\Xi}$ is the $p \times 1$ term that groups all the initial temperature equations $\xi = 0$. Once a valid initial configuration $\mathbf{x}^0$ has been determined, the corresponding initial derivatives $\dot{\mathbf{x}}^0$ can be computed imposing the satisfaction of $\dot{\boldsymbol{\Phi}} = \mathbf{0}$ and the differential equations (3) at time $t = 0$. For the case in which $\dot{\boldsymbol{\rho}}^0 = \mathbf{0}$,

$$\left[\begin{array}{c} \boldsymbol{\Phi}_\mathbf{x} \\ \mathbf{A} \end{array} \right]^0 \dot{\mathbf{x}}^0 = - \left[\begin{array}{c} \boldsymbol{\Phi}_t \\ \mathbf{b} \end{array} \right]^0 \tag{22}$$

In a similar way, the sensitivities of the variables and their derivatives, $\mathbf{x}_{\boldsymbol{\rho}}$ and $\dot{\mathbf{x}}_{\boldsymbol{\rho}}$, must also be compatible with the initial conditions of the LPTN. The initial sensitivity of the variables is obtained from the differentiation of (21) with respect to the system parameters,

$$\left[\begin{array}{c} \boldsymbol{\Phi}_\mathbf{x} \\ \boldsymbol{\Xi}_\mathbf{x} \end{array} \right]^0 \mathbf{x}_{\boldsymbol{\rho}}^0 = - \left[\begin{array}{c} \boldsymbol{\Phi}_{\boldsymbol{\rho}} \\ \boldsymbol{\Xi}_{\boldsymbol{\rho}} \end{array} \right]^0 \tag{23}$$

The differentiation of (22) with respect to $\boldsymbol{\rho}$ provides the initial value of the sensitivity of the derivatives

$$\left[\begin{array}{c} \boldsymbol{\Phi}_\mathbf{x} \\ \mathbf{A} \end{array} \right]^0 \dot{\mathbf{x}}_{\boldsymbol{\rho}}^0 = - \left[\begin{array}{c} \left(\boldsymbol{\Phi}_{\mathbf{x}\mathbf{x}} \mathbf{x}_{\boldsymbol{\rho}} + \boldsymbol{\Phi}_{\mathbf{x}\boldsymbol{\rho}}\right) \dot{\mathbf{x}} + \boldsymbol{\Phi}_{t\mathbf{x}} \mathbf{x}_{\boldsymbol{\rho}} + \boldsymbol{\Phi}_{t\boldsymbol{\rho}} \\ \left(\mathbf{A}_\mathbf{x} \mathbf{x}_{\boldsymbol{\rho}} + \mathbf{A}_{\boldsymbol{\rho}}\right) \dot{\mathbf{x}} + \mathbf{b}_\mathbf{x} \mathbf{x}_{\boldsymbol{\rho}} + \mathbf{b}_{\boldsymbol{\rho}} \end{array} \right]^0 \tag{24}$$

D. Algorithm overview

The steps required by the sensitivity analysis put forward in this Section are summarized in Algorithm 1.

Algorithm 1 Sensitivity analysis procedure

```
t = 0
x ← x^0, ẋ ← ẋ^0                          ▷ Initialize dynamic solver
x_ρ ← x_ρ^0, ẋ_ρ ← ẋ_ρ^0                  ▷ Initialize sensitivities, (23), (24)
while t < t_end do
    t = t + h
    Evaluate residual f, (9)
    while ‖f‖ ≥ tolerance do               ▷ Solve dynamics
        Evaluate tangent matrix df/dx, (10)
        Update variables, (7)
        Evaluate residual f, (9)
    end while
    Evaluate x_ρ, (18)
    Evaluate ẋ_ρ, (16)
end while
```

III. Benchmark problem

A simple RC thermal circuit, introduced in [11] and shown in Fig. 1, was used to benchmark the behaviour of the sensitivity analysis method described in Section II-B.

The circuit features a heat source Q_0 connected to three thermal resistors $R_1 = 1\,\mathrm{K/W}$, $R_2 = 2\,\mathrm{K/W}$, and $R_3 = 3\,\mathrm{K/W}$. Two thermal capacitors, $C_1 = 0.1\,\mathrm{J/K}$ and $C_2 = 0.2\,\mathrm{J/K}$ are connected to nodes 2 and 3 of the circuit, respectively; the initial temperatures of these nodes are set to $T_2^0 = 299\,\mathrm{K}$ and $T_3^0 = 301\,\mathrm{K}$. The temperature of node 4 is constrained to match a fixed value $T_4^\mathrm{f} = 300\,\mathrm{K}$. The benchmark RC thermal circuit can be modelled with a set of $n = 10$ dependent generalized variables $\mathbf{x}$. Of these, four

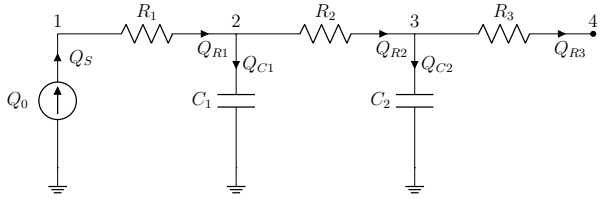

Fig. 1: Benchmark RC thermal circuit

correspond to the temperatures of the nodes and the other six to the heat flows through the components,

$$\begin{aligned} \mathbf{x} &= \left[\begin{array}{cc} \mathbf{x}_T^\mathrm{T} & \mathbf{x}_Q^\mathrm{T} \end{array} \right]^\mathrm{T} \quad \text{where} \\ \mathbf{x}_T &= \left[\begin{array}{cccc} T_1 & T_2 & T_3 & T_4 \end{array} \right]^\mathrm{T} \\ \mathbf{x}_Q &= \left[\begin{array}{cccccc} Q_S & Q_{R1} & Q_{R2} & Q_{R3} & Q_{C1} & Q_{C2} \end{array} \right]^\mathrm{T} \end{aligned} \tag{25}$$

The system dynamics is also described by a set of $r = 9$ parameters $\boldsymbol{\rho}$ that, besides the coefficients of the heat source, the thermal resistors, and the capacitors, includes the fixed temperature of node 4 and the initial temperatures of nodes 2 and 3,

$$\boldsymbol{\rho} = \left[\begin{array}{ccccccccc} Q_0 & R_1 & R_2 & R_3 & C_1 & C_2 & T_4^\mathrm{f} & T_2^0 & T_3^0 \end{array} \right]^\mathrm{T} \tag{26}$$

The variables $\mathbf{x}$ are subjected to the following set of $m = 8$ algebraic constraints

$$\boldsymbol{\Phi} = \left[\begin{array}{c} Q_S - Q_{R1} \\ Q_{R1} - Q_{R2} - Q_{C1} \\ Q_{R2} - Q_{R3} - Q_{C2} \\ T_4 - T_4^\mathrm{f} \\ Q_0 - Q_S \\ T_1 - T_2 - Q_{R1} R_1 \\ T_2 - T_3 - Q_{R2} R_2 \\ T_3 - T_4 - Q_{R3} R_3 \end{array} \right] = \mathbf{0} \tag{27}$$

The first three rows in $\boldsymbol{\Phi}$ stem from Kirchhoff's laws. The fourth equation imposes a constant temperature on node 4. The last four rows correspond to the constitutive relations of

the heat source and the resistors. Moreover, the capacitors in the circuit introduce $p = 2$ differential equations in the form

$$\mathbf{\Gamma} = \begin{bmatrix} Q_{C1} - C_1 \dot{T}_2 \\ Q_{C2} - C_2 \dot{T}_3 \end{bmatrix} = \mathbf{0} \tag{28}$$

A reference solution for this circuit was obtained setting a constant value $Q_0 = 10\,\mathrm{W}$, finding an initial system state compatible with the algebraic and differential constraints and initial conditions, and running a 10-s forward-dynamics simulation, long enough for the system to reach steady-state operation. The evolution of the temperatures and heat flows through the components is shown in Figs. 2 and 3.

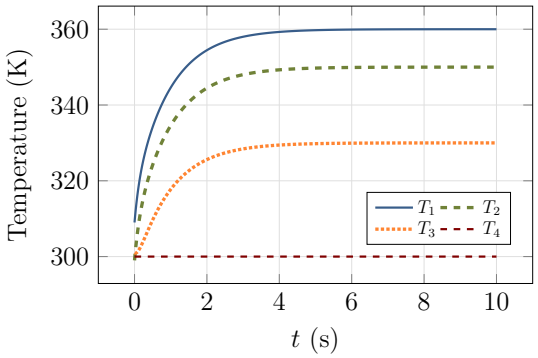

Fig. 2: Temperatures in the simulation of the benchmark circuit.

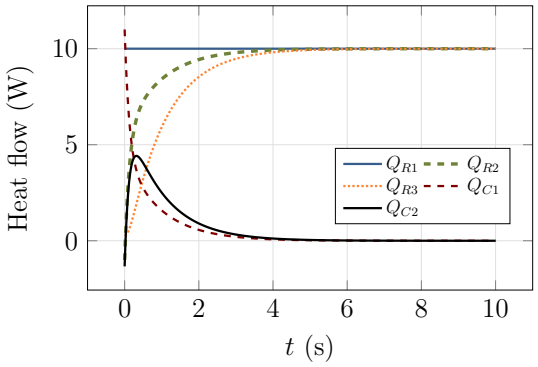

Fig. 3: Heat flows in the simulation of the benchmark circuit.

Figs. 4 and 5 display the sensitivities of the temperature of node 2, T_2, with respect to relevant circuit parameters, namely the values of the thermal resistances and capacitors, evaluated with (18). The shown values agree with the fact that thermal inertias are most relevant during the transient phases, but they have no impact on the steady-state temperatures. Also, the computed sensitivities agree with the expected behaviour of the benchmark circuit; it can be shown that R_1 does not have any effect on T_2, and that at steady state $T_2 = Q_0\,(R_2 + R_3) + T_4^{\mathrm{f}}$.

A. Adjustment of circuit parameters

The sensitivity values $\mathbf{x}_{\boldsymbol{\rho}}$ of the benchmark circuit can be used to perform an optimization of the system parameters from temperature readings from a reference circuit. To this end,

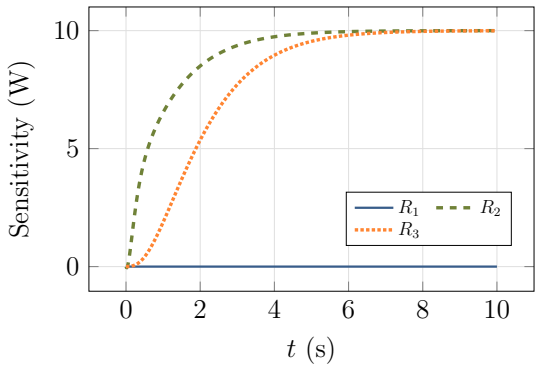

Fig. 4: Sensitivities of the temperature of node 2, T_2, with respect to thermal resistances.

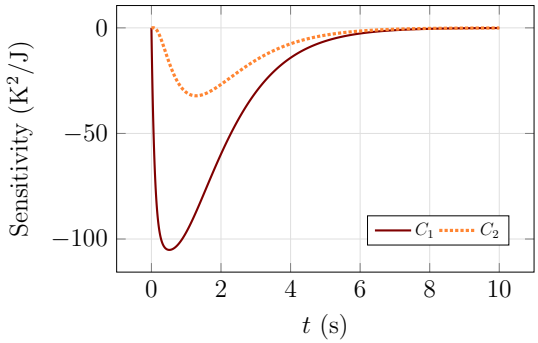

Fig. 5: Sensitivities of the temperature of node 2, T_2, with respect to thermal capacities.

some values in the reference solution circuit were modified to obtain a perturbed system; this perturbed circuit was then adjusted to match the reference values of the original circuit, by means of an optimization process that received as input temperature readings from the ideal benchmark, assumed to be noiseless and accurate. Three optimization scenarios were defined:

- **Case 1**: Adjustment of thermal resistors. The three thermal resistances were modified and set to $R_1^* = 80\,\mathrm{K/W}$, $R_2^* = 20\,\mathrm{K/W}$, and $R_3^* = 50\,\mathrm{K/W}$. Temperature sensors were placed at nodes 1, 2, and 3.
- **Case 2**: Adjustment of thermal capacitors. The thermal capacitances were set to $C_1^* = 2\,\mathrm{J/K}$ and $C_2^* = 5\,\mathrm{J/K}$. Temperature readings from nodes 1 and 2 were used.
- **Case 3**: Adjustment of heat source. A modified value $Q_0^* = 530\,\mathrm{W}$ was set for the perturbed circuit. A temperature sensor was placed at node 1.

The objective function ψ_1 to be minimized in all cases consisted in the square of the differences between sensor readings and model predictions during the duration of a 10-s simulation,

$$\psi_1 = \int_{t^0}^{t^q} \sum_{i=1}^{s} \left(T_i - \hat{T}_i\right)^2 \mathrm{d}t \tag{29}$$

where s is the number of sensors used in each scenario, T_i is the temperature in the reference circuit, obtained through the ideal sensor i, and $\hat{T}_i$ is the temperature at the same location predicted by the perturbed circuit. The integral in (29) was

evaluated in a discrete form, and temperatures were sampled every 0.001 s. A Levenberg-Marquardt (LM) optimization scheme [24], [25], [26], an algorithm that belongs to the nonlinear least squares solution family, was used to conduct the parameter adjustment in the defined cases.

The optimization procedure consisted in an iterative process that started with the execution of the 10-s forward-dynamics simulation and the evaluation of the sensitivities with the method described in Section II-B. Next, the objective function ψ_1 and its gradient $\psi_{1\boldsymbol{\rho}}$ were evaluated using the time-history of the system variables and their sensitivities, and updated values of the benchmark parameters were obtained by means of the LM algorithm. The process was repeated until the value of the objective function went below a threshold. Because the temperatures T_i retrieved by the ideal sensors were not affected by noise, the stopping criterion was set to $\psi_1 = 10^{-10}$ K^2, a rather stringent condition.

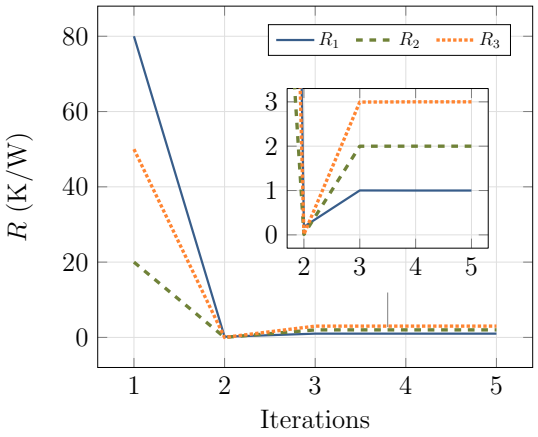

Fig. 6: Benchmark problem: convergence of resistances in scenario 1.

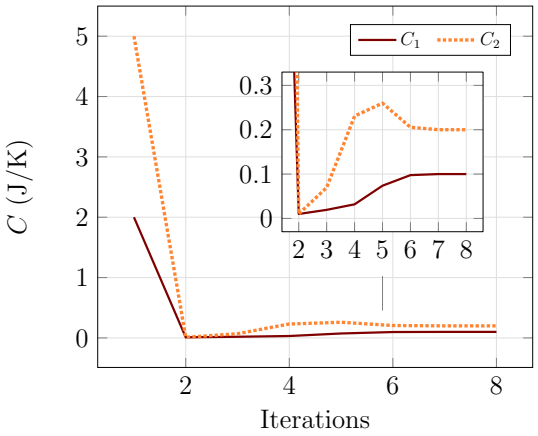

Fig. 7: Benchmark problem: convergence of capacitances in scenario 2.

Fig. 6 shows the convergence of the resistance values during the optimization process in scenario 1. Even though the initial parameters differed from the correct ones by an order of magnitude, the algorithm converged in five iterations. In fact, after three steps the difference between the obtained values and the reference was less than 0.2% of the correct value. A similar behaviour was observed during the adjustment of the thermal capacitors in scenario 2. Again, the initial values C_1^* and C_2^* were an order of magnitude larger than the reference values. The method converged to the correct capacitances in eight iterations, as shown in Fig. 7. The tuning of the heat source parameter Q_0 in case 3 required three iterations of the method as confirmed by Fig. 8, starting from a value that was fifty times larger than the correct one. These results confirmed the suitability of analytically evaluated sensitivities to be used in optimization algorithms for the adjustment of LPTNs, provided that an appropriate number of sensor measurements are available to guide the optimization process.

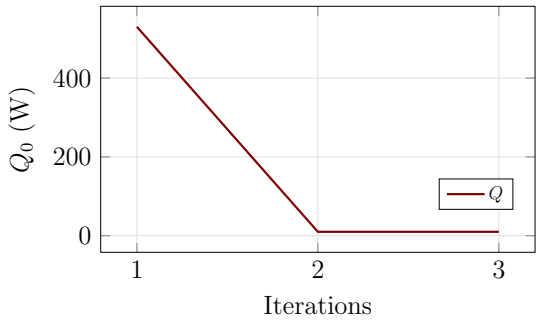

Fig. 8: Benchmark problem: convergence of heat source in scenario 3.

IV. Industrial Example: ePowertrain Motor

The sensitivity analysis method presented in Section II-B was also evaluated in the calibration process of the LPTN of an automotive-grade PMSM. The following main parts were identified in the eMotor topology: shaft, bearings, rotor, magnets, end-plates, end-rings, stator iron, active winding, endwindings, housing with heat extraction sinks, cooling jacket, and internal air cavities. These are shown in Fig. 9 together with the heat paths between them; dashed and solid lines represent convection and conduction, respectively.

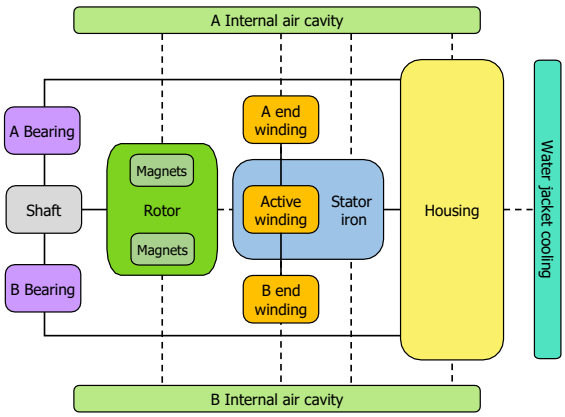

Fig. 9: eMotor LPTN modular scheme.

The LPTN consists in a 23-node, 60 components network. Its initial lumped parameters (R, C) were estimated based

on material properties and motor geometry. Heat sources were modeled using commercial multi physics simulation software. The model includes 13 heat sources to account for the electromagnetic and mechanical energy losses in the motor, 22 constant-value resistors to represent heat transfer by conduction, 15 variable resistors to represent convection, and 10 thermal capacitors. The dependence of the heat losses with component temperature was considered in this study; however, the thermal resistance and capacity of the circuit elements were treated as independent from their temperatures.

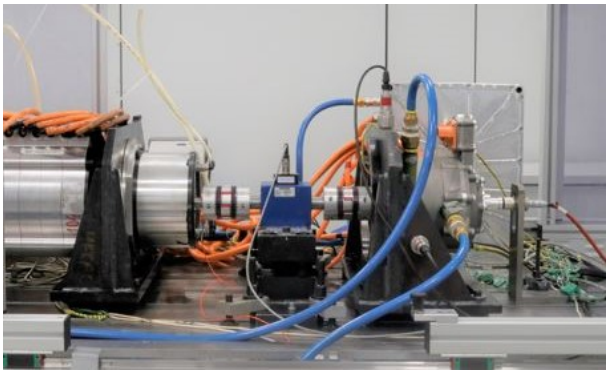

Fig. 10: Testing of the eMotor in a bench.

In order to verify the goodness of fit for the initial LPTN model, the motor was mounted on a test bench as shown in Fig. 10. The two eMotors rest on a metallic base platform, assembled in a back-to-back configuration, mechanically coupled by a torque sensor between their shafts. Two commercial inverters are used to control the motors commanding speed or torque to each of them. The communication between the inverters and the eMotors is performed by a commercial controller via controller area network (CAN) protocol. The tested motor was subjected to a WLTP (Worldwide Harmonised Light Vehicles Test Procedure) cycle, a commonly used 1800-s long homologation test [27]. The angular speed and torque of the selected eMotor during this cycle are shown in Figs. 11 and 12.

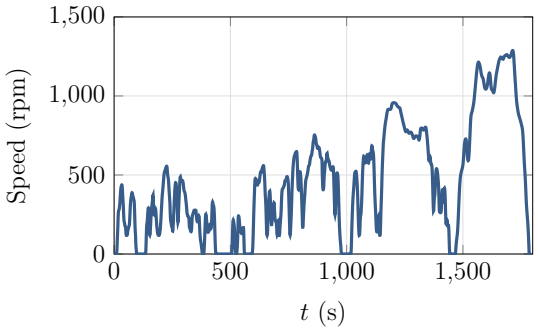

Fig. 11: Speed of the eMotor during the WLTP cycle.

Type K thermocouples were used to measure temperatures at 3 locations: the rotor magnets and the A and B endwindings. Sixteen sensors were installed in the stator, in the locations shown in Fig. 13. Besides, eight thermocouples were placed

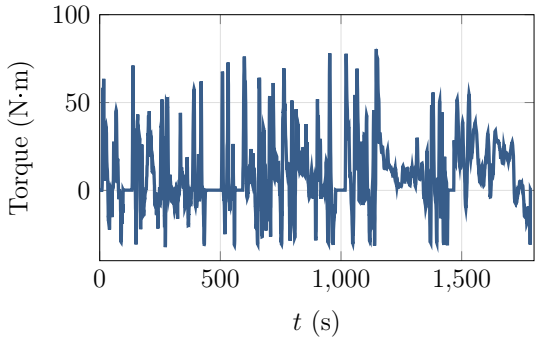

Fig. 12: Torque of the eMotor during the WLTP cycle.

in the rotor in two different stacks, as presented in Fig. 14. Data from the latter are retrieved by means of a commercial wireless system consisting of two parts: emitter and receiver. The emitter is introduced in the shaft cavity, connected to the thermocouples at the measurement points, and rotates solidary to the rotor. The receiver is static and is separated by an air gap from the emitter and retrieves the data wirelessly.

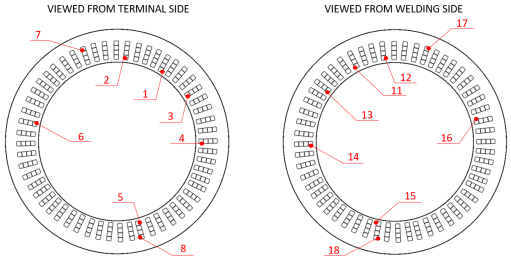

Fig. 13: Location of the sensors in the stator: B-side endwinding (left) and A-side endwinding (right).

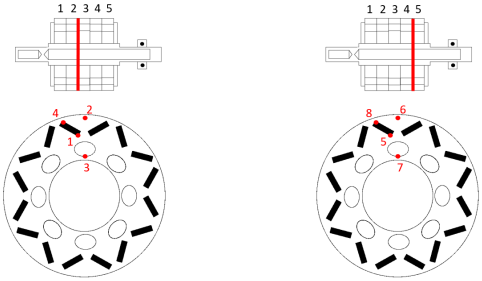

Fig. 14: Location of the sensors in the rotor.

In order to illustrate the ability of the formulation in Section II-B to determine the sensitivities of the system variables with respect to its parameters, the thermal dynamics of the eMotor LPTN was simulated during the test cycle. The procedure was then repeated adding the evaluation of the sensitivity of the 20 temperatures and 60 heat flows in the circuit with respect to its 73 parameters, which included thermal loss values Q, the resistance R and capacity C parameters of the components, the initial temperatures of the capacitors, and the fixed temperatures at those points of the LPTN that represent refrigerant fluid temperatures.

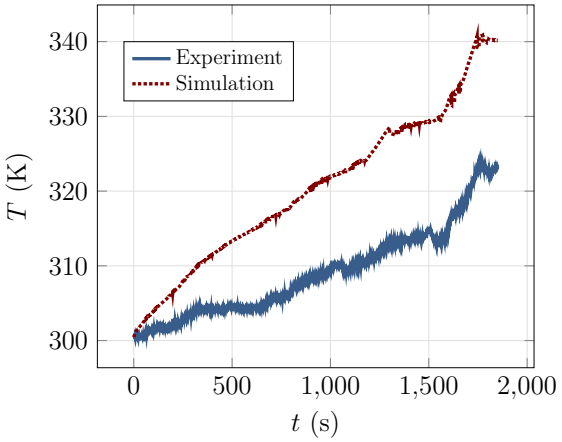

Fig. 15: Magnet temperatures during the WLTP cycle: comparison of experiments and initial simulation results.

The experimental results confirmed the existence of differences between the predictions of the LPTN of the eMotor and the sensor readings. Fig. 15 shows that the initial simulation results regarding magnet temperatures differ up to 20 K from the sensor readings at that location. These differences remained below 12 K for the sensors placed at the endwindings.

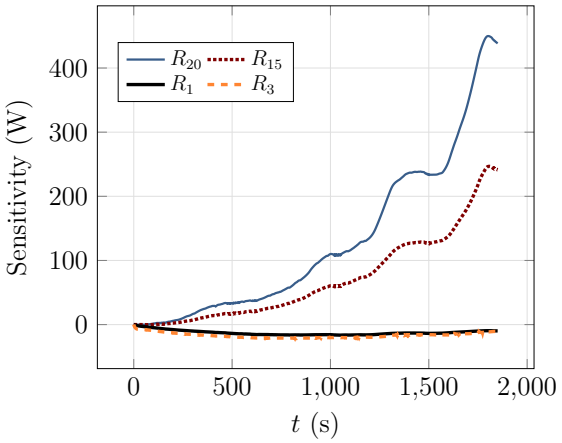

Fig. 16: Sensitivity of magnet temperature during the WLTP cycle with respect to conduction resistances.

The formulation in Section II-B was used to determine the sensitivities of the 20 temperatures and 60 heat flows in the circuit with respect to the 73 parameters in the LPTN. Figs. 16 and 17 show the sensitivity of the magnet temperature with respect to the most critical system parameters. The plots in Fig. 16 represent the sensitivity of this temperature with respect to conduction resistances. Terms R_{15} and R_{20} stand for the resistance associated to the thermal paths between the stator teeth and yoke, and between the stator and its housing, respectively. Terms R_1 and R_3 are located between the magnets and the rotor axis. The capacities to which Fig. 17 refers are related to the rotor axis (C_2), the rotor (C_{27}) and the endwindings (C_{78} and C_{81}). Figs. 16 and 17 highlight the fact that sensitivities vary considerably depending on the operation point of the motor; for instance, the resistance of the thermal

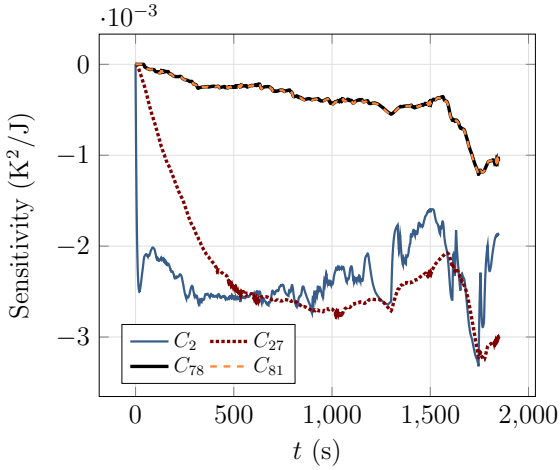

Fig. 17: Sensitivity of magnet temperature during the WLTP cycle with respect to thermal capacitors.

TABLE II: Operation speeds during continuous service tests.

Test	1	2	3	4	5	6
ω (rpm)	3500	4000	6000	7000	8000	9000

path between the stator teeth and the refrigerant fluid becomes more relevant during the last stages of the WLTP cycle, when the motor operates under more demanding conditions.

In the light of the results of the sensitivity analysis, four LPTN parameters were selected as target for optimization, namely resistances R_{20} and R_{15}, corresponding to the heat flow path between the stator teeth and the water jacket, and capacities C_{27} and C_2, that represent the thermal inertia of the rotor and its shaft, respectively.

The optimization procedure adjusted the values of these four parameters using the sensor data obtained during a series of continuous service tests, during which the motor was commanded to operate at a fixed angular speed while exerting a constant torque value, until its internal temperatures reached a steady state. The operation speeds ω of the performed tests are shown in Table II. Temperature readings for these experiments were gathered from the same locations as in the initial WLTP cycle.

Each continuous service experiment was simulated using the dynamic formulation in Section II-A; a sensitivity analysis was performed simultaneously with the formulation in Section II-B. The obtained results were used to determine the Jacobian matrix of an objective function consisting in the aggregate of the squared differences between sensor readings and simulation results of the six experiments in Table II,

$$\psi_{\text{cs}} = \sum_{j=1}^{6} \int_{t^0}^{t_j^q} \sum_{i=1}^{s} \left(T_{i,j} - \hat{T}_{i,j} \right)^2 \mathrm{d}t \tag{30}$$

where $T_{i,j}$ denotes the reading of sensor i during experiment j and $\hat{T}_{i,j}$ is the corresponding simulation result. The number of sensors was $s = 3$. The problem was optimized by means of a constrained Levenberg-Marquardt algorithm. The variation of each tuned parameter with respect to its initial value was

penalized when it exceeded a factor of 3 or 1/3, in order to prevent the optimized solution to drift too far from the initial estimation, which corresponded to physical calculations. The iteration process of the algorithm was stopped when the variation of the square root of ψ_{cs} dropped below a value of 10 K over a window of ten consecutive iteration steps. The algorithm converged after 16 iterations. Then, the WLTP cycle was repeated with the adjusted LPTN parameters.

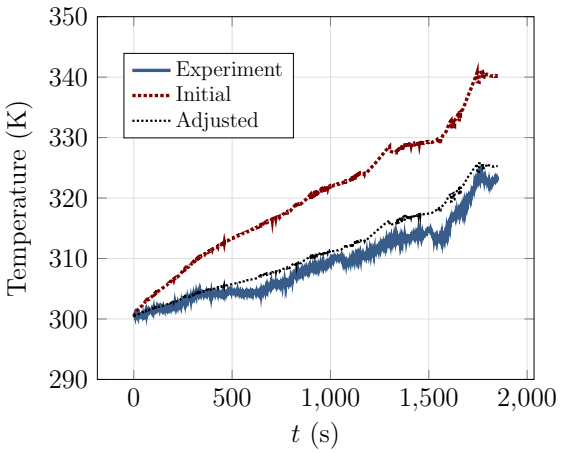

Fig. 18: Temperature of the magnets during the WLTP cycle.

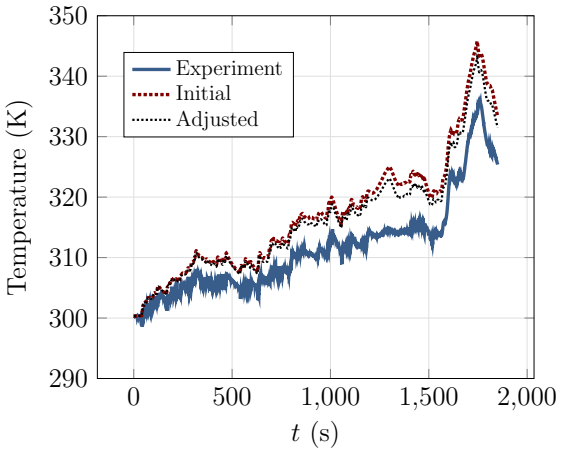

Fig. 19: Temperature of the B endwinding during the WLTP cycle.

Figs. 18 and 19 compare the experimental temperatures at the magnets and the B endwinding to those delivered by simulation with the initial and adjusted LPTN. Results for the A endwinding showed a similar behaviour to those of its B counterpart. The differences between sensor readings and simulation descended below 5 K at the magnets, as shown in Fig. 20. The agreement also improved at the endwindings, although moderately, as confirmed by Fig. 21. This stems from the fact that only the most critical parameters for the temperature of the magnets were chosen as optimization targets; even though, the overall LPTN implementation benefited from the optimization, as confirmed by the endwinding results.

It must be stressed that other optimization schemes, different from the one here proposed, could have been used to adjust

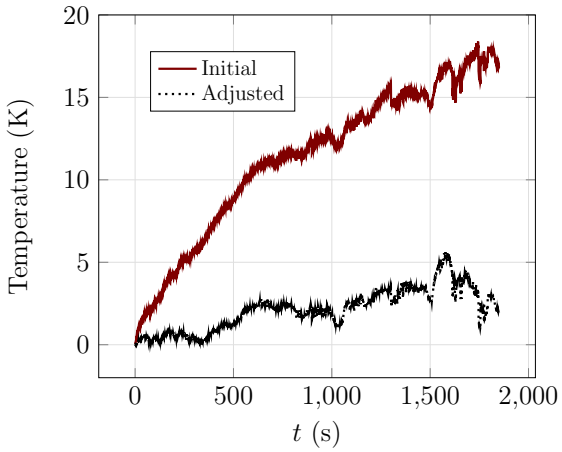

Fig. 20: Differences between sensor readings and simulation at the magnets in the WLTP cycle.

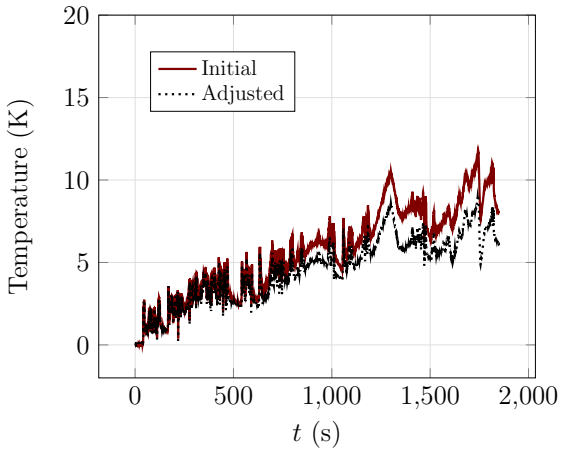

Fig. 21: Differences between sensor readings and simulation at the B endwinding in the WLTP cycle.

the parameters of the motor LPTN. The method reported in this Section is meant to confirm the ability of the analytical sensitivities here presented to be used as input for the gradient-based optimization of thermal circuits; these sensitivities can be evaluated at a reduced computational cost with the exact formulation introduced in Section II-B.

V. Discussion

The proposed sensitivity method was compared to a finite-differences approach, a commonly used solution in the literature for sensitivity computation, e.g., [12], [28], in terms of efficiency and accuracy. The dynamic simulation was repeated introducing a perturbation in each of the parameters of the LPTN. The sensitivity of each variable was evaluated as the difference between its values in the original and the perturbed simulation, divided by the value of the perturbation. In the benchmark circuit, the sensitivities of its ten variables were calculated with respect to the nine parameters of the model. For the motor LPTM, sensitivities of all variables were calculated with respect to the constant parameters alone: 22 resistors and 10 capacitors.

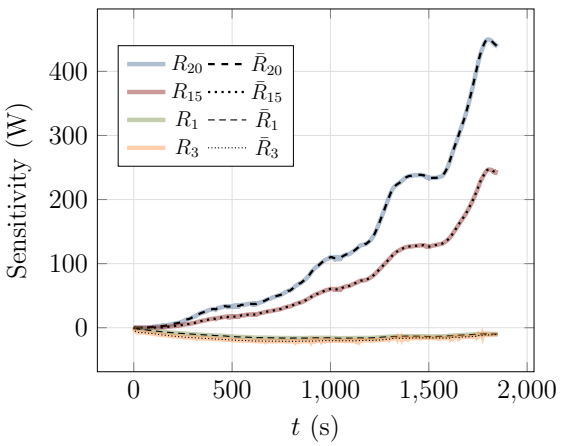

Fig. 22: Analytical (R) and finite-difference ($\bar{R}$) sensitivity of the magnet temperature in the PMSM with respect to conduction resistances.

TABLE III: Maximum differences between analytical and finite-difference sensitivity of temperature T_2 in the benchmark problem with respect to LPTN parameters.

Param.	R_1	R_2	R_3	C_1	C_2
	0 W	10^{-5} W	10^{-5} W	10^{-3} K²/J	10^{-4} K²/J

Fig. 22 compares the sensitivity of the magnet temperature in the PMSM model obtained by both methods, with respect to resistance values. A similar agreement was obtained for the sensitivities with respect to capacitances, also with the benchmark problem. Tables III and IV show the maximum differences between the sensitivities delivered by both methods in the benchmark and the PMSM analysis.

In order to assess their computational efficiency, the simulation and sensitivity analysis methods were coded in C++, compiled with GNU gcc 11.3.0, and run in a desktop computer with an AMD Ryzen 5 5600X 6-core processor and 16GB RAM, running Ubuntu 22.04. The integration step-sizes were $h = 0.001$ s and $h = 0.5$ s for the benchmark and the PMSM, respectively. The elapsed times are shown in Table V.

TABLE IV: Maximum differences between analytical and finite-difference sensitivity of the magnet temperature in the PMSM with respect to LPTN parameters.

Parameter	R_{20}	R_{15}	R_3	R_1
Difference (W)	0.59	0.31	$2.6 \cdot 10^{-3}$	$3.0 \cdot 10^{-3}$
Parameter	C_2	C_{27}	C_{81}	C_{78}
Difference (K²/J)	$1.9 \cdot 10^{-6}$	$2.4 \cdot 10^{-6}$	$5.3 \cdot 10^{-6}$	$3.9 \cdot 10^{-6}$

TABLE V: Elapsed times in the computation of the dynamics simulation and the sensitivity analysis of the examples.

	Dynamics	Sensitivity	Finite differences
Benchmark circuit (10 s)	0.023 s	0.062 s	0.345 s
Motor circuit (1800 s)	0.112 s	1.041 s	3.076 s

TABLE VI: Maximum difference between finite-difference and analytical sensitivity of the magnet temperature with respect to R_{20} in the PMSM model, for different values of the perturbation δR in the finite differences method.

δR (K/W)	1	10^{-3}	10^{-6}	10^{-9}	10^{-12}	10^{-15}
Difference (W)	403.10	4.31	0.59	0.59	2.63	648.06

The use of analytical sensitivities features two important advantages with respect to finite differences: it is computationally advantageous and it removes the need to select the numerical differentiation approach and perturbation size to arrive perform the analysis. As an example, Table VI shows the difference between analytical and finite differences results caused by the use of different perturbation sizes in the evaluation of the sensitivity of the magnet temperature with respect to R_{20} in the PMSM model. The perturbation size must remain within a certain, a priori unknown range to avoid numerical issues. The use of analytical sensitivities does not suffer from this problem.

VI. Conclusions

The sensitivity analysis of lumped-parameter thermal networks (LPTN) can be conducted in an accurate and efficient way by means of the evaluation of the analytical sensitivities of the system variables with respect to the model parameters. This approach is computationally advantageous when compared to strictly numerical methods and does not rely on perturbations of the initial solution. Moreover, it provides an expression of the evolution of the sensitivity as the system dynamics progresses in time.

In this work, a formulation for the sensitivity analysis of LPTN models has been put forward. This method is based upon the expression of the thermal dynamics of the circuit as a system of differential-algebraic equations and its integration by means of BDF. The ability of the sensitivity formulation to deliver a meaningful prediction of the evolution of the system sensitivities over time was evaluated by means of a benchmark RC thermal circuit and the LPTN representation of a permanent-magnet synchronous motor. Moreover, the obtained sensitivity values were used as input for optimization algorithms during the adjustment of the model parameters. In the case of the RC benchmark, the parameters were tuned to match those of a known computational model. For the PMSM model, representative thermal resistance and inertia values were modified to capture the thermal behaviour of the motor during experimental tests that consisted in continuous service and WLTP cycles. Results confirmed that the sensitivity method is able to correctly capture the effect of the variations of the system parameters; additionally, the computation of sensitivities takes place at a minimal computational cost and can be conducted simultaneously with the integration of the circuit dynamics.

References

[1] P. Milanfar and J. Lang, "Monitoring the thermal condition of permanent-magnet synchronous motors," *IEEE Transactions on Aerospace and Electronic Systems*, vol. 32, no. 4, pp. 1421–1429, 1996.

[2] A. A. López, D. J. B. Smith, and B. Mecrow, "Magnet loss reduction: A new technique beyond segmentation and shielding," in *11th International Conference on Power Electronics, Machines and Drives (PEMD 2022)*, Newcastle, UK, 2022.

[3] W. Li, Z. Cao, and X. Zhang, "Thermal analysis of the solid rotor permanent magnet synchronous motors with air-cooled hybrid ventilation systems," *IEEE Transactions on Industrial Electronics*, vol. 69, no. 2, pp. 1146–1156, 2021.

[4] M. Sumislawska, K. N. Gyftakis, D. F. Kavanagh, M. McCulloch, K. J. Burnham, and D. A. Howey, "The impact of thermal degradation on electrical machine winding insulation," in *2015 IEEE 10th International Symposium on Diagnostics for Electrical Machines, Power Electronics and Drives (SDEMPED)*. Guarda, Portugal: IEEE, 2015.

[5] V. Madonna, P. Giangrande, and M. Galea, "Influence of insulation thermal aging on the temperature assessment in electrical machines," *IEEE Transactions on Energy Conversion*, vol. 36, no. 1, pp. 456–467, 2021.

[6] A. Boglietti, A. Cavagnino, D. Staton, M. Shanel, M. Mueller, and C. Mejuto, "Evolution and modern approaches for thermal analysis of electrical machines," *IEEE Transactions on Industrial Electronics*, vol. 56, no. 3, pp. 871 – 882, 2009.

[7] K. Wu, L. Cai, J. Zhang, Y. Fang, and Y. Wang, "Thermal analysis of deep-sea oil-filled motor using lumped-parameter thermal model and CFD," in *2022 IEEE Transportation Electrification Conference and Expo, Asia-Pacific (ITEC Asia-Pacific)*, Haining, China, 2022.

[8] B. Rodríguez, F. González, M. Á. Naya, and J. Cuadrado, "Assessment of methods for the real-time simulation of electronic and thermal circuits," *Energies*, vol. 13, no. 6, p. paper 1354, 2020.

[9] O. Wallscheid and J. Böcker, "Fusion of direct and indirect temperature estimation techniques for permanent magnet synchronous motors," in *2017 IEEE International Electric Machines and Drives Conference (IEMDC)*, Miami, FL, USA, 2017.

[10] P. N. Phuc, D. Bozalakov, H. Vansompel, K. Stockman, and G. Crevecoeur, "Rotor temperature virtual sensing for induction machines using a lumped-parameter thermal network and dual Kalman filtering," *IEEE Transactions on Energy Conversion*, vol. 36, no. 3, pp. 1688–1699, sep 2021.

[11] B. Rodríguez, E. Sanjurjo, M. Tranchero, C. Romano, and F. González, "Thermal parameter and state estimation for digital twins of e-powertrain components," *IEEE Access*, vol. 9, pp. 97 384–97 400, 2021.

[12] U. Abubakar, X. Wang, S. H. Shah, and S. Ur rahman, "Parametric thermal sensitivity analysis of 225kW high speed PMSM for blower application," in *IEEE Industrial Electronics and Applications Conference (IEACon)*, Penang, Malaysia, 2021.

[13] B. Assaad, K. El kadri Benkara, S. Vivier, G. Friedrich, and A. Michon, "Thermal design optimization of electric machines using a global sensitivity analysis," *IEEE Transactions on Industry Applications*, vol. 53, pp. 5365–5372, 2017.

[14] O. Wallscheid and J. Bocker, "Global identification of a low-order lumped-parameter thermal network for permanent magnet synchronous motors," *IEEE Transactions on Energy Conversion*, vol. 31, no. 1, pp. 354–365, 2016.

[15] G. G. Guemo, P. Chantrenne, and J. Jac, "Parameter identification of a lumped parameter thermal model for a permanent magnet synchronous machine," in *2013 International Electric Machines & Drives Conference*, Chicago, IL, USA, 2013, pp. 1316–1320.

[16] F. Zhang, D. Gerada, Z. Xu, H. Zhang, and C. Gerada, "Sensitivity analysis of machine components thermal properties effects on winding temperature," in *2019 22nd International Conference on Electrical Machines and Systems (ICEMS)*, Harbin, China, 2019.

[17] D. Dopico, Y. Zhu, A. Sandu, and C. Sandu, "Direct and adjoint sensitivity analysis of ordinary differential equation multibody formulations," *Journal of Computational and Nonlinear Dynamics*, vol. 10, no. 1, 2014.

[18] J. R. R. A. Martins, P. Sturdza, and J. J. Alonso, "The complex-step derivative approximation," *ACM Transactions on Mathematical Software*, vol. 29, no. 3, pp. 245–262, sep 2003.

[19] C. E. Christoffersen, "Implementation of exact sensitivities in a circuit simulator using automatic differentiation," in *Proceedings of ECMS 20th European Conference on Modelling and Simulation*, W. Borutzky, A. Orsoni, and R. Zobel, Eds., Bonn, Germany, 2006.

[20] A. Callejo, S. H. K. Narayanan, J. G. de Jalón, and B. Norris, "Performance of automatic differentiation tools in the dynamic simulation of multibody systems," *Advances in Engineering Software*, vol. 73, pp. 35–44, 2014.

[21] B. Minaker and F. González, "Automatic differentiation in automatic generation of the linearized equations of motion," in *17th International Conference on Multibody Systems, Nonlinear Dynamics, and Control (MSNDC)*, vol. 9, Online event, 2021, pp. DETC2021–69 118.

[22] D. Dopico, F. González, A. Luaces, M. Saura, and D. García-Vallejo, "Direct sensitivity analysis of multibody systems with holonomic and nonholonomic constraints via an index-3 augmented Lagrangian formulation with projections," *Nonlinear Dynamics*, vol. 93, pp. 2040–2056, 2018.

[23] E. Hairer, S. P. Nørsett, and G. Wanner, *Solving Ordinary Differential Equations I*. Berlin, Germany: Springer, 1993.

[24] K. Levenberg, "A method for the solution of certain non-linear problems in least squares," *Quarterly of Applied Mathematics*, vol. 2, no. 2, pp. 164–168, 1944.

[25] D. W. Marquardt, "An algorithm for least-squares estimation of non-linear parameters," *Journal of the Society for Industrial and Applied Mathematics*, vol. 11, no. 2, pp. 431–441, 1963.

[26] R. Fletcher, "A modified Marquardt subroutine for non-linear least squares," United Kingdom Atomic Energy Authority, Tech. Rep., 1971.

[27] United Nations, "Global technical regulation 15, Worldwide harmonized Light vehicles Test Procedure (ECE/trans/180/add.15)," Tech. Rep., 2014.

[28] Q. Ai, H. Wei, H. Dou, W. Zhao, and Y. Zhang, "Robust rotor temperature estimation of permanent magnet motors for electric vehicles," *IEEE Transactions on Vehicular Technology*, vol. 72, no. 7, pp. 8579–8591, 2023.